

---

# AlphaNet: Scaling Up Local Frame-based Neural Network Interatomic Potentials

---

<b>Bangchen Yin</b> <sup>*</sup> Tsinghua University	<b>Jiaao Wang</b> <sup>*†</sup> UT Austin	<b>Weitao Du</b> DAMO Academy	<b>Pengbo Wang</b> HKUST
<b>Penghua Ying</b> Tel Aviv University	<b>Haojun Jia</b> Deep Principle, Inc.	<b>Zisheng Zhang</b> Stanford University	<b>Yuanqi Du</b> <sup>†</sup> Cornell University
<b>Carla P. Gomes</b> Cornell University	<b>Graeme Henkelman</b> UT Austin	<b>Chenru Duan</b> <sup>†</sup> Deep Principle, Inc.	<b>Hai Xiao</b> <sup>†</sup> Tsinghua University

## Abstract

Molecular dynamics simulations demand unprecedented accuracy and scalability to tackle grand challenges in energy materials, catalytic processes, and biomolecular design. To bridge this gap, we present AlphaNet, a local frame-based equivariant model that simultaneously advances computational efficiency and predictive precision for atomistic systems. By constructing equivariant local frames with learnable geometric transitions, AlphaNet encodes atomic environments with enhanced representational capacity, achieving state-of-the-art accuracy in energy and force predictions. Extensive benchmarks—spanning defected graphene, formate decomposition, inorganic bulks, and large-scale datasets (OC2M and Matbench Discovery) demonstrate its superior performance over existing neural network interatomic potentials while ensuring scalability across diverse system sizes. The synergy of accuracy, efficiency, and transferability positions AlphaNet as a transformative tool for simulating multiscale phenomena, from catalyst dynamics to energy storage interfaces, with direct implications for accelerating the discovery of functional materials and complex molecular systems. Our code and data is available at <https://github.com/zmyybc/AlphaNet>.

## 1 Introduction

Molecular dynamics (MD) simulations have become essential for exploring and understanding complex phenomena in areas such as energy storage, catalysis, and biological systems (Richards et al., 2016; Boero et al., 1998; Lindorff-Larsen et al., 2011). While atomic forces necessary for these simulations can be derived from quantum mechanical approaches such as density functional theory (DFT), the computational cost associated with such first-principles methods severely limits their application to small-sized systems ( $\sim 10^3$  atoms) and short timescales ( $\sim 10^1$  ps). As a result, a wide spectrum of phenomena occurring over much larger scales remain inaccessible, even with the most powerful supercomputers.

Classical force fields, which rely on predefined mathematical forms, offer a computationally efficient alternative, allowing simulations of larger systems over extended trajectories (Jones and Chapman, 1924; Cornell et al., 1995; MacKerell et al., 1998). However, the simplicity of these models often

---

<sup>\*</sup>These authors contributed equally to this work.

<sup>†</sup>Corresponding authors. Emails: wangjiaao0720@utexas.edu, yuanqidu@cs.cornell.edu, duanchenru@gmail.com and haixiao@tsinghua.edu.cn.

compromises their accuracy, leading to a trade-off between computational speed and the fidelity of the simulated dynamics (Iftimie et al., 2005).

The advent of machine learning techniques has introduced a promising solution to this dilemma. By training models on data derived from first-principles calculations, neural network interatomic potentials (NNIPs) can potentially achieve the accuracy of first-principles methods while maintaining the computational efficiency of classical force fields. Unlike traditional models that rely on explicit functional forms to describe the bonded and non-bonded interactions, NNIPs are more flexible, learning to predict interactions based on the positions of atoms and their chemical identities.

As interest in applying NNIPs to large-scale atomistic systems continues to grow, the field has seen a surge in the development of various innovative models. One example among the others, DPA-1 (Zhang et al., 2024a), is a large-scale pre-trained model with improved attention architecture over DeepPot (Wang et al., 2018). Similarly, JMP (Shoghi et al., 2024) leverages diverse molecular systems of different types as a joint pre-training model. MACE (Batatia et al., 2022), on the other hand, introduces higher-order message passing as a complete basis of many-body atomic interactions. Collectively, these models represent significant strides in the evolution of NNIP-driven atomistic simulations (Qu and Krishnapriyan, 2024; Liao et al., 2024; Gasteiger et al., 2021; Batzner et al., 2022; Schütt et al., 2018; Smith et al., 2017; Deng et al., 2023).

Nevertheless, the balance between computational efficiency and accuracy is key to the practical application of these models. On one side, efficient yet less expressive models are more suitable for tasks that weigh computational cost more than accuracy. On the other side, less efficient yet expressive models are more suitable for tasks where accuracy is more important. Atomistic systems in 3D Euclidean space are invariant to Euclidean symmetries including rotation, translation and reflection. Thus, equivariant models are developed to respect these symmetries (Satorras et al., 2021; Thomas et al., 2018), and most of these expressive models by date (Batzner et al., 2022; Batatia et al., 2022; Liao et al., 2024) are based on the spherical harmonics (Geiger and Smidt, 2022), but calculating the tensor product of irreducible representations imposes expensive computational overheads. While another branch of work achieves rotation equivariance through building equivariant frames that can be either local or global (Jumper et al., 2021; Du et al., 2022, 2023; Duval et al., 2023), and the main benefit of frame-based approaches is eliminating the necessity to involve the tensor product, thus greatly improving the computational efficiency.

In this paper, we propose a local-frame-based equivariant atomistic model, named AlphaNet, for accurate yet highly efficient atomistic simulations. Building on the success of frame-based NNIPs in small atomistic systems, we introduce an additional rotary positional embedding to enhance the frame transition and temporal connection for multi-scale modeling. Extensive quantitative experiments demonstrate that AlphaNet excels at accuracy, efficiency and scalability compared with the state-of-the-art (SOTA) NNIP models on a variety of systems, ranging from defected graphenes, formate decomposition, zeolites, surface reactions and inorganic bulks.

## 2 Results

We systematically assess the capabilities of AlphaNet by examining its prediction accuracy, scalability with respect to model and dataset size, and computational efficiency in terms of inference speed and memory usage. Initially, we validate atomic-level prediction accuracy across five diverse chemical systems, simultaneously demonstrating AlphaNet’s scalability concerning dataset and system sizes. Subsequently, we quantify computational efficiency by benchmarking both the memory footprint and inference costs of the model. Comprehensive details regarding datasets, comparative methodologies, and hyperparameter configurations are provided in Appendix B.

### 2.1 AlphaNet achieving high accuracy across all datasets.

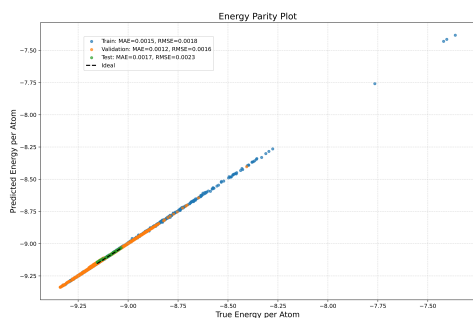
We first consider the formate decomposition dataset, which serves as a representative example of catalytic surface reactions, specifically focuses on the dehydrogenation of formate ( $\text{HCOO}^* \rightarrow \text{H}^* + \text{CO}_2$ ) on a Cu  $\langle 110 \rangle$  surface. For this dataset, AlphaNet achieves a mean absolute error (MAE) of 45.5 meV/Å for force and 0.23 meV/atom for energy, compared to NequIP (Batzner et al., 2022) 47.3 meV/Å and 0.50 meV/atom, respectively, as shown in Table 1. These results underscore AlphaNet’s ability to effectively capture the intricate nature of heterogeneous systems, which often involve both

metallic and covalent bonding, along with complex charge transfer processes between the metal and adsorbed molecules. This high degree of accuracy highlights the model’s suitability for simulating catalytic reactions with multiple interaction types.

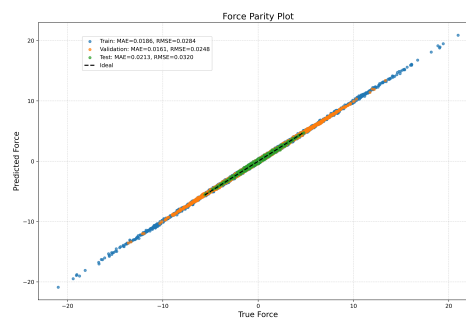
Another challenge for NNIP models is accurately modeling the sliding layer effect in materials like defected graphene, where inter-layer interactions are critical. On the defected graphene dataset, AlphaNet achieves a force MAE of 32.0 meV/Å and an energy MAE of 1.7 meV/atom, substantially outperforming NequIP, which records 60.2 meV/Å for force MAE and 1.9 meV/atom for energy MAE. Furthermore, AlphaNet successfully reproduces the binding energy curve for AB-stacked bilayer graphene as calculated by PBE+MBD, without requiring explicit long-range dispersion interaction corrections. The deviation in the shallow sliding potential energy landscape is less than 0.4 meV/atom, illustrating AlphaNet’s capacity to handle systems with subtle interlayer forces and complex structural dynamics (as shown in Figure 1).

Table 1: Results on the Formate Decomposition and Defected Graphene datasets. Boldface indicates the best performance.

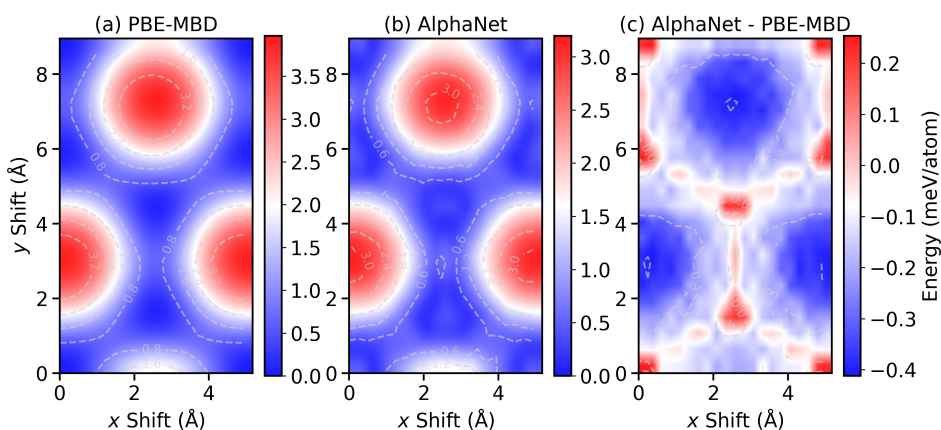
Dataset	Metric	NequIP	AlphaNet
<b>Formate Decomposition</b>	Force MAE (meV/Å) ↓	47.3	<b>45.5</b>
	Energy MAE (meV/atom) ↓	0.50	<b>0.23</b>
<b>Defected Graphene</b>	Force MAE (meV/Å) ↓	60.2	<b>32.0</b>
	Energy MAE (meV/atom) ↓	1.9	<b>1.7</b>



(a) Parity plot for total energies obtained for the training (blue), validation (orange), and test (green) data sets.



(b) Parity plot for atomic forces obtained for the training (blue), validation (orange), and test (green) data sets.



(c) AlphaNet (middle) and DFT (left) sliding PES for bilayer graphene, and their difference (right).

Figure 1: Comparisons between AlphaNet predictions and DFT calculations on the Zeolite dataset.

The third dataset we consider is the zeolite dataset, comprising 16 types of zeolites and a total of 800,000 configurations. Table 2 shows the results of Deep Pot (Wang et al., 2018) and AlphaNet across different zeolite configurations. Across nearly all tested configurations, AlphaNet significantly outperforms Deep Pot in both energy and force predictions. For instance, in the ABWopt configuration, AlphaNet achieves an Energy MAE of 41 meV, substantially lower than Deep Pot’s 90 meV. Similarly, AlphaNet records a Force MAE of 54 meV/Å, outperforming Deep Pot’s 90 meV/Å.

Table 2: Results on the Zeolite dataset. Boldface indicates the best performance. (Unit for energy is meV/atom and unit for force is meV/Å).

Metric	ABWopt		BCTopt		BPHopt		CANopt	
	Deep Pot	AlphaNet	Deep Pot	AlphaNet	Deep Pot	AlphaNet	Deep Pot	AlphaNet
Energy MAE ↓	90	<b>71</b>	110	<b>73</b>	210	<b>41</b>	150	<b>62</b>
Force MAE ↓	90	<b>54</b>	<b>50</b>	55	<b>60</b>	90	90	<b>10</b>
Metric	EDIOpt		FERopt		GISopt		JBWopt	
	Deep Pot	AlphaNet	Deep Pot	AlphaNet	Deep Pot	AlphaNet	Deep Pot	AlphaNet
Energy MAE ↓	40	<b>5.4</b>	290	<b>100</b>	60	<b>56</b>	150	<b>18</b>
Force MAE ↓	50	<b>59</b>	130	<b>18</b>	50	<b>3.1</b>	70	<b>50</b>
Metric	LOSOpt		LTAopt		LTJopt		NATOpt	
	Deep Pot	AlphaNet	Deep Pot	AlphaNet	Deep Pot	AlphaNet	Deep Pot	AlphaNet
Energy MAE ↓	<b>110</b>	130	150	<b>90</b>	70	<b>1.2</b>	210	<b>47</b>
Force MAE ↓	70	<b>46</b>	64	<b>60</b>	110	<b>60</b>	110	<b>9.9</b>
Metric	PARopt		PHIOpt		SODOpt		THOopt	
	Deep Pot	AlphaNet	Deep Pot	AlphaNet	Deep Pot	AlphaNet	Deep Pot	AlphaNet
Energy MAE ↓	90	<b>6.5</b>	60	<b>16</b>	200	<b>9.5</b>	160	<b>70</b>
Force MAE ↓	70	<b>3.5</b>	120	<b>50</b>	110	<b>21</b>	60	<b>47</b>

Table 3: Results on the OC20 validation set. “full” denotes models trained on the full OC20 training set, others are trained on the 2M subset.  $\lambda_E$  refers to the weight of the energy loss, the weight of the force loss  $\lambda_F$  is set to 100. Boldface indicates the best performance.

Model	Parameters ↓	Energy MAE (eV) ↓	Force MAE (eV/Å) ↓
SchNet (full)	9.1M	0.54	0.55
DimeNet++ (full)	10.1M	0.53	0.048
GemNet	38M	0.29	0.026
eSCN	51M	0.28	0.021
EScAIP-Medium	146M	0.25	<b>0.019</b>
EquiformerV2 ( $\lambda_E = 2$ )	146M	0.28	0.022
AlphaNet ( $\lambda_E = 4$ )	<b>6.1M</b>	0.25	0.040
AlphaNet ( $\lambda_E = 20$ )	<b>6.1M</b>	<b>0.24</b>	0.062

The next challenge, we consider the Open Catalyst Project OC20 dataset (Chanussot et al., 2021), a comprehensive collection of crystal structures for training NNIP models in catalysis. We focus on the subset OC2M and the Structure-to-energy-and-force (S2EF) task. We compare the performance of our model against established benchmarks, including EquiformerV2 (Liao et al., 2024), EScAIP (Qu and Krishnapriyan, 2024), eSCN (Passaro and Zitnick, 2023), GemNet-OC (Gasteiger et al., 2022), SchNet (Schütt et al., 2018), and DimeNet++ (Gasteiger et al., 2020).

AlphaNet, trained on the 2M subset for 2,000,000 steps, achieves exceptional accuracy in energy prediction, with a mean absolute error (MAE) of 0.24 eV. This performance is comparable to larger models like EquiformerV2 and EScAIP, while SchNet and DimeNet++, trained on the full dataset, exhibit worse MAE values (>0.35 eV). However, AlphaNet trained on the 2M subset does not outperform larger models like EquiformerV2 and EScAIP in the force prediction task. This may be attributed to the **conservativeness** of the models, which ensures forces are derived as  $-\nabla_x E(x)$ .

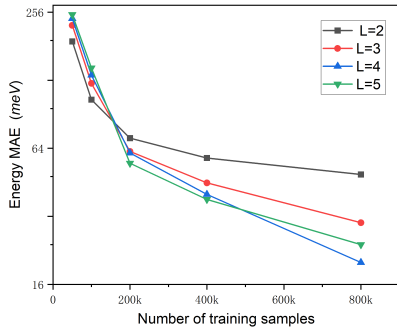
Table 4: Results on the Matbench Discovery WBM unique prototype dataset. Boldface indicates the best performance.

Model	F1 $\uparrow$	DAF $\uparrow$	Prec $\uparrow$	Acc $\uparrow$	MAE $\downarrow$	R2 $\uparrow$	Size $\downarrow$	Type
CHGNet	0.613	3.361	0.514	0.851	0.063	0.689	413k	EFSGM
MACE-MP-0	0.669	3.777	0.577	0.878	0.057	0.697	4.69M	EFSG
GRACE-2L-MPtrj	0.691	4.163	0.636	0.896	0.052	0.741	15.3M	EFSG
SevenNet-0	0.724	4.252	0.65	0.904	0.048	0.75	842k	EFSG
SevenNet-13i5	0.76	4.629	0.708	0.92	0.044	0.776	1.17M	EFSG
ORB MPtrj	0.765	4.702	0.719	0.922	0.045	0.756	25.2M	EFSD
DPA3-v1-MPtrj	0.765	4.654	0.711	0.921	0.042	0.798	3.37M	EFSG
eqV2 S DeNS	0.815	5.042	0.771	0.941	0.036	0.788	31.2M	EFSD
EScAIP-Small	0.782	5.634	0.712	0.939	0.038	0.783	45M	EFSD
AlphaNet	0.799	4.863	0.743	0.933	0.041	0.745	16.2M	EFSG

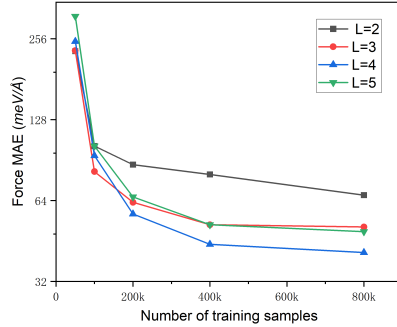
For the last challenge, we validate the effectiveness of AlphaNet on the well-established Matbench discovery WBM test set (Riebesell et al., 2024), AlphaNet demonstrates a compelling balance between accuracy and physical consistency on the WBM benchmark 4. With a 0.799 F1 score and 4.863 DAF score, it achieves near state-of-the-art classification performance while employing an *EFSG-type conservative force field* that rigorously enforces physical constraints. Notably, its compact architecture (16.2M parameters) outperforms the 31.2M-parameter *eqV2 S DeNS* model in regression tasks ( $R^2 = 0.742$ ) with lower prediction error (MAE = 0.039). This combination of efficiency and physics-aware design positions AlphaNet as a robust NNIP model for scalable materials modeling.

## 2.2 AlphaNet is scalable—effective scaling with both model, data and system sizes

In addition to maintaining high performance with large datasets and large systems, we validate the scaling of model size and dataset size on the zeolite dataset. We can observe the performance improves as the training data size increases from 50k to 800k samples, as shown in Figure 2. Specifically, the energy MAE decreases from 220 meV at 50k samples to 41 meV at 800k samples. Similarly, the force MAE decreases from 241 meV/Å at 5k samples to 54 meV/Å at 80k samples. Furthermore, deeper neural networks improve performance faster with the growth of the dataset size. This trend highlights the scalability of AlphaNet with increasing dataset size and model size.



(a) Energy MAE (meV) vs Data Size



(b) Force MAE (meV/Å) vs Data Size

Figure 2: Mean absolute errors of energy and force predictions of models with  $L$  number of layers as a function of training data size on the zeolite dataset.

## 2.3 AlphaNet is efficient—achieves the best speed-accuracy trade-off

The primary advantage of NNIP models over density functional theory (DFT) calculated energy and force lies in their significantly faster inference speed. Although increasing the number of parameters

in an NNIP model generally enhances its performance, this often comes at the cost of slower inference speed. To evaluate the speed of different NNIPs, we evaluate the average forward pass time across 2,000 zeolite structures with a batch size of 10. In addition, we test systems of varying sizes by expanding the unit cells. Although we aim to maintain a consistent number of parameters across models, slight variations exist due to different components in each model (detailed in Appendix B.4).

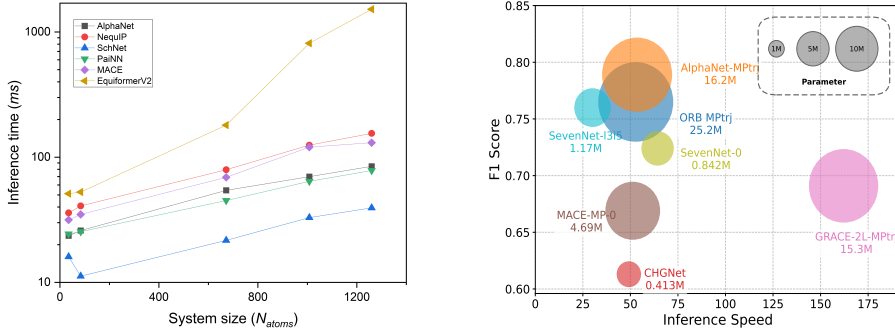


Figure 3: Comparisons of inference speed among various NNIP models. (a) Inference speed as a function of system size. The x-axis represents the number of atoms in the system, and the y-axis shows the average time required to predict energy and forces for systems in batches of 10, across a total of 200 batches on the Zeolite dataset. (b) Inference speed, F1 performance and model size of models accessible and compliant with the Matbench Discovery leaderboard. The speed is calculated as the number of energy evaluation per second.

As illustrated in Figure 3 (a), AlphaNet demonstrates a distinct speed advantage over other NNIP models, exhibiting a relatively slow increase in computational time as the size of the system increases. This indicates that AlphaNet’s speed scales efficiently with larger systems, making it a more suitable option for handling increasing system sizes.

Furthermore, we evaluated the inference speed of the pre-trained models on the Matbench Discovery leaderboard (Riebesell et al., 2024). To ensure fairness, we select models that are compliant, open-source, and accessible without additional requests. We evaluate the average speed of energy prediction and present in Figure 3 (b). The models included AlphaNet, ORB-v2 (Neumann et al., 2024), SevenNet (Park et al., 2024), GRACE (Bochkarev et al., 2024), MACE (Batatia et al., 2022), and CHGNet (Deng et al., 2023). Among these models, GRACE, developed based on TensorFlow, exhibits remarkable speed compared to the others, which are PyTorch-based. Notably, AlphaNet-MPtrj’s inference speed is comparable to models with 10 times fewer parameters (e.g., SevenNet-13i5). This suggests that AlphaNet achieves competitive efficiency despite its larger parameter count, and it would be intriguing to explore its performance with fewer parameters in future work.

Table 5: Efficiency evaluated on the OC20 dataset, using a single A100 40GB GPU. Conserv. denotes energy conservation. Boldface indicates the best performance.

Models	Parameters ↓	Training Speed (Sample/Sec) ↑	Training Memory (GB/Sample) ↓	Inference Speed (Sample/Sec) ↑	Inference Memory (GB/Sample) ↓	Conserv.
SchNet	9.1M	39	2.5	112.1	1.7	✓
DimeNet++	10.1M	29	3.6	92	2.5	✓
GemNet-OC	38M	16.22	1.63	39.2	1.61	×
eSCN	51M	8.5	1.75	25.2	1.74	×
EScAIP	83M	37.8	<b>1.23</b>	111.8	<b>1.09</b>	×
EquiformerV2	31M	15.7	1.63	36.72	1.61	×
AlphaNet	<b>6.1M</b>	<b>41.2</b>	2.2	<b>120.1</b>	1.5	✓

The last efficiency evaluation is on the OC20 dataset, as shown in Table 5. Notably, EScAIP demonstrates remarkable efficiency in both speed and memory usage despite its large size, while AlphaNet shows a slight advantage in inference speed but consumes more memory than it. It is important to note that models such as AlphaNet, SchNet, and DimeNet++ are conservative, meaning

their force calculations inherently require additional computational resources for PyTorch autograd, resulting in higher inference time and memory costs.

### 3 Discussion

AlphaNet presents a significant advancement as a scalable neural network interatomic potential, offering both high precision and fast computational speed. This success can be attributed to its local-frame-based architecture, which scalarizes geometric quantities over local frames and effectively aggregate local frames to construct local- and global-aware features. By utilizing this architecture, our model excels at capturing complex interactions across a broad spectrum of systems, including metallic, covalent, and ionic bonding, as well as long-range interactions.

One of the key advantages of AlphaNet lies in its scalability. Specifically, our model is capable of maintaining high performance as both the size of the dataset and size of the atomic systems increase. Despite the growing complexity introduced by larger datasets, AlphaNet operates with fewer parameters, making it more efficient while still delivering robust results. This ability to handle large datasets without sacrificing accuracy positions AlphaNet as a promising solution for extensive simulations and real-world applications.

For future work, we aim to extend the model’s capabilities to explore additional types of interactions, such as hydrogen bonding, which are critical in a wide range of chemical and biological systems. Furthermore, the interpretability of the proposed model is worth exploring. While our current implementation achieves impressive results, gaining a deeper understanding of how the model interprets and processes interactions at the atomic level will enhance its applicability and trustworthiness in practical scenarios. There is another long-term challenge: the efficient use of GPU memory during training, particularly when dealing with large systems consisting of over 1,000 atoms (though we can parallelize it across multiple GPUs). This is a common limitation shared by most message-passing neural networks, and addressing it will be crucial for enabling the model to scale further in both size and complexity. Future work will focus on optimizing memory usage to overcome this bottleneck and ensure the model’s applicability to even larger systems.

### 4 Methodology

**Neural Network Interatomic Potentials.** A single state of a molecular system can be described by a set of atom types  $h \in \mathbb{R}^{n \times d}$  and atomic positions  $x \in \mathbb{R}^{n \times 3}$ . In molecular dynamics, we are interested in learning a function  $f : \mathbb{R}^{n \times d} \times \mathbb{R}^{n \times 3} \rightarrow \mathbb{R}$  which predicts the energy of the current state of the molecular system readily to be used for simulation. The force can be further calculated by  $-\nabla_x f(x)$ , thus often referred as to neural network interatomic potentials (NNIPs).

**Message-passing neural networks.** One common way to model molecular systems is through message-passing neural networks, which is a general neural architecture that leverages both permutation equivariance and locality in graph-structured data. Specifically, there are two essential operations in message-passing neural networks, message calculation and message update. The message calculation operation encodes structured messages from local environments  $m_i = \oplus_{j \in \mathcal{N}(i)} f_m(f_h(x_i), h(x_j), e_{ij})$  where  $i$  and  $j$  denotes the index of different nodes,  $e_{ij}$  denotes optional edge features and  $f_m$  and  $f_h$  denotes neural networks that encode both edge and node features; The message update aggregates the incoming messages from the neighbors  $m_i = f_u(m_i)$ , where  $f_u$  is a neural network.

**Equivariant message-passing neural networks.** Equivariance is another crucial property to building MLFFs as molecular systems are invariant to the Euclidean group. A function  $f$  is said to be equivariant with respect to certain group  $G$  if  $f \circ g(x) = g \circ f(x), \forall x \in X, g \in G$ . One natural property of message-passing neural networks is the permutation equivariance such that changing the order of the input set of nodes do not result in difference output for the same node as it only depends on the neighbors which are unchanged under permutation. In addition to permutation, we need to consider the special Euclidean group in 3D, SE(3), which includes rotation and translation operations. We do so by leveraging local frames (Du et al., 2022). Specifically, we build a set of equivariant and complete frames and scalarize the geometric quantity which does not break SE(3)-equivariance under nonlinear neural network encodings.

To build equivariant and complete frames from atomic positions, we consider the following edge-based frames following (Du et al., 2022):

$$\mathcal{F}_{ij} = (\hat{e}_{ij}^1, \hat{e}_{ij}^2, \hat{e}_{ij}^3) = \left( \frac{x_i - x_j}{\|x_i - x_j\|}, \frac{(x_i - \bar{x}) \times (x_j - \bar{x})}{\|(x_i - \bar{x}) \times (x_j - \bar{x})\|}, \frac{(x_i - x_j) \times ((x_i - \bar{x}) \times (x_j - \bar{x}))}{\|(x_i - x_j) \times ((x_i - \bar{x}) \times (x_j - \bar{x}))\|} \right)$$

To scalarize geometric quantity such as a vector  $v$ , we take the inner product between it and the frames which results in a set of invariant scalars and can be inverted via a tensorization operation

$$\begin{aligned} \text{Scalarize}(v, \mathcal{F}_{ij}) &= (s_{ij}^1, s_{ij}^2, s_{ij}^3) = (e_{ij}^1 \cdot v, e_{ij}^2 \cdot v, e_{ij}^3 \cdot v) \\ \text{Tensorize}(s_{ij}, \mathcal{F}_{ij}) &= s_{ij}^1 e_{ij}^1 + s_{ij}^2 e_{ij}^2 + s_{ij}^3 e_{ij}^3 \end{aligned}$$

**Efficient and expressive equivariant message-passing neural networks.** Following (Du et al., 2024), we leverage an efficient and expressive extension of the above equivariant message-passing neural networks based on local frames. We consider two modules to improve the expressiveness while maintaining the efficiency of the network. Specifically, we leverage a local structure encoding module which scalarizes not only features from local neighbors but also from overlapping neighbors along each edge, denoted as  $A_{ij} := f_l(\text{Scalarize}(S_{i-j}, \mathcal{F}_{ij}))$ , where  $f_l$  denotes a neural network and  $S_{i-j}$  represents overlapping neighbors of node  $i$  and  $j$ . In addition, we use an additional frame transition module which encodes the alignment between each neighboring frame to improve the expressiveness. We realize this by incorporating vector-based message passing to amortize the cost where  $\mathbf{m}_{ij}$  denotes equivariant edge features. This framework is highly efficient as it avoids expensive higher-body message-passing neural networks and higher-order tensor updates.

$$\{h_i, x_i\} = \{f_u(\oplus_{j \in \mathcal{N}(i)} f_m(h(x_i), h(x_j), A_{ij}, e_{ij})), \oplus_{j \in \mathcal{N}(i)} f_m(h(x_i), h(x_j), A_{ij}, e_{ij}) \mathbf{m}_{ij})\}$$

**Rotary positional embedding as invariant frame transition.** Positional embedding are known to improve and stabilize the training of transformers (Shaw et al., 2018). We introduce the elegant relationship between the commonly used Rotary Position Embedding (RoPE) and frame transition we use in our architecture (Su et al., 2024). In fact the frame transition can be considered as a generalized rotary positional embedding for 3D equivariant frames. Note that the spirit of rotary position embedding is to design an embedding scheme for relative position in sequential data. To build the rotary positional embedding, (Su et al., 2024) utilizes the relative index between nodes  $x_i$  and  $x_j$  of a one-dimensional sequence to find a function  $g(x_i, x_j, i - j)$  such that

$$\langle f_q(x_i, i), f_k(x_j, j) \rangle = g(x_i, x_j, i - j)$$

where  $f_q$  and  $f_k$  denote the neural network embeddings of query and key inside an attention layer. Fortunately, there is an explicit way of building  $g$  by multiplying  $f_{\{q,k\}}(x_i, i)$  with the diagonal matrix expanded by rotation matrices (Su et al., 2024):

$$\begin{pmatrix} \cos \theta_n & -\sin \theta_n \\ \sin \theta_n & \cos \theta_n \end{pmatrix}$$

where  $\theta_n = 10000^{-2 \frac{(n-1)}{d}}$ ,  $n \in [1, 2, \dots, \frac{d}{2}]$ , and  $d$  is the dimension of features. From a geometric point of view, the index  $i$  of  $x_i$  provides a one-dimensional position embedding such that the inner product  $\langle f_q(x_i, i), f_k(x_j, j) \rangle$  only depend on the relative position  $i - j$ . In the three-dimensional world, we can utilize the frame transition matrices between  $x_i$  and  $x_j$  that plays a similar rule of the index difference  $i - j$  in a one-dimensional sequence. In addition, we introduce the rotary positional embedding on invariant features  $h$  and represent the rotation by the multiplication of complex numbers. We predict an additional complex number from our invariant features  $h_i$  for each node  $i$  and multiply it by the scalarized features  $h_i$ . Similar to the equivariant message passing in each layer of the network, the learned rotary embedding is also applied in each layer.

**Temporal connection.** In addition to commonly adapted message passing in the spatial domain, we consider another dimension, temporal domain, which can be described by the depth of the neural network (Chen et al., 2018). As message-passing neural networks are local, we believe it is beneficial to integrate multi-scale information. Specifically, for each consecutive layer, we learn a kernel that linear transforms and aggregates features. Given the invariant feature embeddings  $h^{l_1}$  at layer  $l_1$  and  $h^{(l_2)}$  at layer  $l_2$ , the kernel is of the matrix product form:  $M^{(l_3, 1, 2)}$  which transforms  $h^{(l_1)}$  and  $h^{(l_2)}$  to a new feature  $h^{(l_3)}$  and added as a residual into the next layer:

$$h^{(l_3)} = \sum_{k_1=1}^{K_1} \left( \sum_{k_2=1}^{K_2} M_{k_1, k_2}^{(l_3, 1, 2)} \cdot h_{k_2}^{(l_2)} \right) \cdot h_{k_1}^{(l_1)}$$



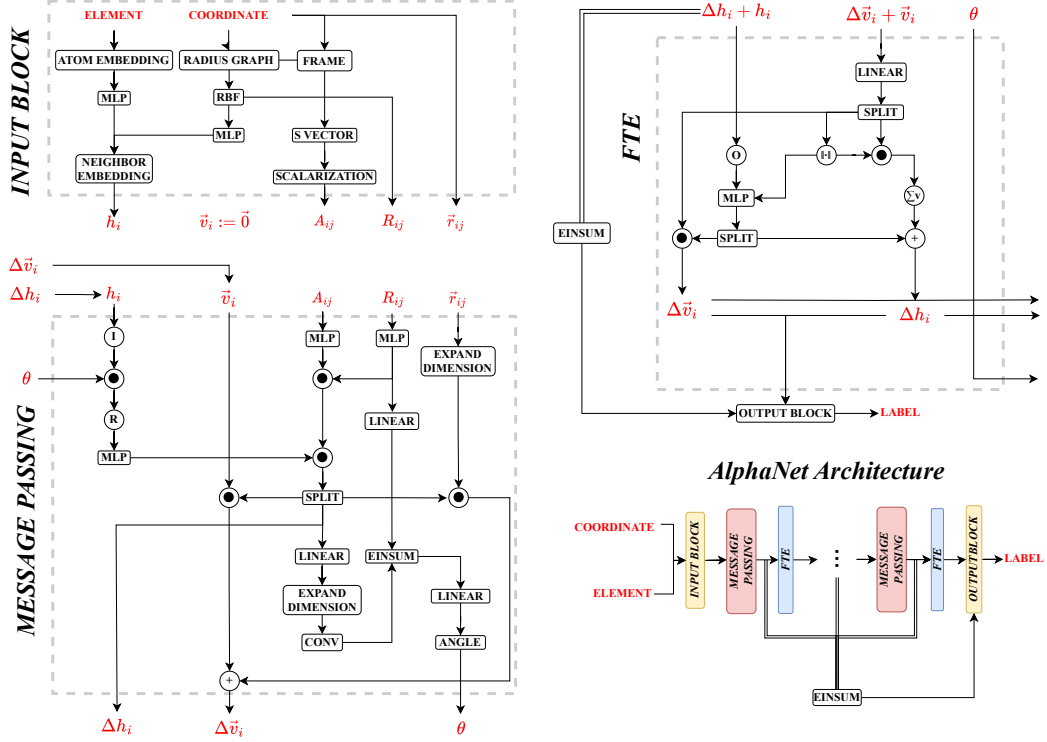


Figure 4: Overview of AlphaNet framework. We first process the input atomic types and coordinates to scalarized features and frames and pass them further to a loop of message passing and frame transition layers, followed by an output block with a temporal connection to the final output.  $I/R$  denotes imaginary and real number,  $\|\bullet\|$  denotes norm,  $\bullet$  denotes element-wise multiplication, and  $\circ$  denotes vector scaling.

## References

- I. Batatia, D. P. Kovacs, G. N. C. Simm, C. Ortner, and G. Csanyi. MACE: Higher order equivariant message passing neural networks for fast and accurate force fields. In A. H. Oh, A. Agarwal, D. Belgrave, and K. Cho, editors, *Advances in Neural Information Processing Systems*, 2022. URL <https://openreview.net/forum?id=YppSngE-ZU>.
- S. Batzner, A. Musaelian, L. Sun, M. Geiger, J. P. Mailoa, M. Kornbluth, N. Molinari, T. E. Smidt, and B. Kozinsky. E(3)-equivariant graph neural networks for data-efficient and accurate interatomic potentials. *Nature Communications*, 13(1):2453, 2022. doi: 10.1038/s41467-022-29939-5.
- A. Bochkarev, Y. Lysogorskiy, and R. Drautz. Graph atomic cluster expansion for semilocal interactions beyond equivariant message passing. *Phys. Rev. X*, 14:021036, Jun 2024. doi: 10.1103/PhysRevX.14.021036. URL <https://link.aps.org/doi/10.1103/PhysRevX.14.021036>.
- M. Boero, M. Parrinello, and K. Terakura. First principles molecular dynamics study of ziegler natta heterogeneous catalysis. *Journal of the American Chemical Society*, 120(12):2746–2752, 1998. doi: 10.1021/ja972367i. URL <https://doi.org/10.1021/ja972367i>.
- R. Car and M. Parrinello. Unified approach for molecular dynamics and density-functional theory. *Phys. Rev. Lett.*, 55:2471–2474, Nov 1985. doi: 10.1103/PhysRevLett.55.2471. URL <https://link.aps.org/doi/10.1103/PhysRevLett.55.2471>.
- L. Chanussot, A. Das, S. Goyal, T. Lavril, M. Shuaibi, M. Riviere, K. Tran, J. Heras-Domingo, C. Ho, W. Hu, A. Palizhati, A. Sriram, B. Wood, J. Yoon, D. Parikh, C. L. Zitnick, and Z. Ulissi. Open catalyst 2020 (oc20) dataset and community challenges. *ACS Catalysis*, 11(10):6059–6072, May 2021. ISSN 2155-5435. doi: 10.1021/acscatal.0c04525. URL <http://dx.doi.org/10.1021/acscatal.0c04525>.

- R. T. Chen, Y. Rubanova, J. Bettencourt, and D. K. Duvenaud. Neural ordinary differential equations. *Advances in neural information processing systems*, 31, 2018.
- W. D. Cornell, P. Cieplak, C. I. Bayly, I. R. Gould, K. M. Merz, D. M. Ferguson, D. C. Spellmeyer, T. Fox, J. W. Caldwell, and P. A. Kollman. A second generation force field for the simulation of proteins, nucleic acids, and organic molecules. *Journal of the American Chemical Society*, 117(19):5179–5197, 1995. doi: 10.1021/ja00124a002. URL <https://doi.org/10.1021/ja00124a002>.
- B. Deng, P. Zhong, K. Jun, et al. Chgnet as a pretrained universal neural network potential for charge-informed atomistic modelling. *Nature Machine Intelligence*, 5:1031–1041, 2023. doi: 10.1038/s42256-023-00716-3. URL <https://doi.org/10.1038/s42256-023-00716-3>.
- W. Du, H. Zhang, Y. Du, Q. Meng, W. Chen, N. Zheng, B. Shao, and T.-Y. Liu. Se (3) equivariant graph neural networks with complete local frames. In *International Conference on Machine Learning*, pages 5583–5608. PMLR, 2022.
- W. Du, Y. Du, L. Wang, D. Feng, G. Wang, S. Ji, C. P. Gomes, and Z.-M. Ma. A new perspective on building efficient and expressive 3d equivariant graph neural networks. In *Thirty-seventh Conference on Neural Information Processing Systems*, 2023. URL <https://openreview.net/forum?id=hWPNYwkYPN>.
- Y. Du, L. Wang, D. Feng, G. Wang, S. Ji, C. P. Gomes, Z.-M. Ma, et al. A new perspective on building efficient and expressive 3d equivariant graph neural networks. *Advances in Neural Information Processing Systems*, 36, 2024.
- A. A. Duval, V. Schmidt, A. Hernández-García, S. Miret, F. D. Malliaros, Y. Bengio, and D. Rolnick. FAENet: Frame averaging equivariant GNN for materials modeling. In A. Krause, E. Brunskill, K. Cho, B. Engelhardt, S. Sabato, and J. Scarlett, editors, *Proceedings of the 40th International Conference on Machine Learning*, volume 202 of *Proceedings of Machine Learning Research*, pages 9013–9033. PMLR, 23–29 Jul 2023. URL <https://proceedings.mlr.press/v202/duval23a.html>.
- J. Gasteiger, J. Groß, and S. Günnemann. Directional message passing for molecular graphs. In *International Conference on Learning Representations (ICLR)*, 2020.
- J. Gasteiger, F. Becker, and S. Günnemann. Gemnet: Universal directional graph neural networks for molecules. *Advances in Neural Information Processing Systems*, 34:6790–6802, 2021.
- J. Gasteiger, M. Shuaibi, A. Sriram, S. Günnemann, Z. W. Ulissi, C. L. Zitnick, and A. Das. Gemnet-OC: Developing graph neural networks for large and diverse molecular simulation datasets. *Transactions on Machine Learning Research*, 2022. ISSN 2835-8856. URL <https://openreview.net/forum?id=u8tvSxm4Bs>.
- M. Geiger and T. Smidt. e3nn: Euclidean neural networks, 2022. URL <https://arxiv.org/abs/2207.09453>.
- G. Henkelman, B. P. Uberuaga, and H. Jónsson. A climbing image nudged elastic band method for finding saddle points and minimum energy paths. *The Journal of Chemical Physics*, 113(22): 9901–9904, 12 2000. ISSN 0021-9606. doi: 10.1063/1.1329672. URL <https://doi.org/10.1063/1.1329672>.
- R. Iftimie, P. Minary, and M. E. Tuckerman. Ab initio molecular dynamics: Concepts, recent developments, and future trends. *Proceedings of the National Academy of Sciences*, 102(19): 6654–6659, 2005.
- J. E. Jones and S. Chapman. On the determination of molecular fields. —ii. from the equation of state of a gas. *Proceedings of the Royal Society of London. Series A, Containing Papers of a Mathematical and Physical Character*, 106(738):463–477, 1924. doi: 10.1098/rspa.1924.0082. URL <https://royalsocietypublishing.org/doi/abs/10.1098/rspa.1924.0082>.
- J. Jumper, R. Evans, A. Pritzel, et al. Highly accurate protein structure prediction with alphafold. *Nature*, 596:583–589, 2021. doi: 10.1038/s41586-021-03819-2. URL <https://doi.org/10.1038/s41586-021-03819-2>.

- G. Kresse and J. Furthmüller. Efficient iterative schemes for ab initio total-energy calculations using a plane-wave basis set. *Phys. Rev. B*, 54:11169–11186, Oct 1996. doi: 10.1103/PhysRevB.54.11169. URL <https://link.aps.org/doi/10.1103/PhysRevB.54.11169>.
- G. Kresse and J. Hafner. Ab initio molecular dynamics for open-shell transition metals. *Phys. Rev. B*, 48:13115–13118, Nov 1993. doi: 10.1103/PhysRevB.48.13115. URL <https://link.aps.org/doi/10.1103/PhysRevB.48.13115>.
- T. D. Kühne, M. Iannuzzi, M. D. Ben, V. V. Rybkin, P. Seewald, F. Stein, T. Laino, R. Z. Khaliullin, O. Schütt, F. Schiffmann, D. Golze, J. Wilhelm, S. Chulkov, M. H. Bani-Hashemian, V. Weber, U. Borštnik, M. TAILLEFUMIER, A. S. Jakobovits, A. Lazzaro, H. Pabst, T. Müller, R. Schade, M. Guidon, S. Andermatt, N. Holmberg, G. K. Schenter, A. Hehn, A. Bussy, F. Belleflamme, G. Tabacchi, A. Glöß, M. Lass, I. Bethune, C. J. Mundy, C. Plessl, M. Watkins, J. VandeVondele, M. Krack, and J. Hutter. CP2k: An electronic structure and molecular dynamics software package - quickstep: Efficient and accurate electronic structure calculations. *The Journal of Chemical Physics*, 152(19):194103, May 2020. doi: 10.1063/5.0007045. URL <https://doi.org/10.1063/5.0007045>.
- Y.-L. Liao, B. M. Wood, A. Das, and T. Smidt. Equiformerv2: Improved equivariant transformer for scaling to higher-degree representations. In *The Twelfth International Conference on Learning Representations*, 2024.
- K. Lindorff-Larsen, S. Piana, R. O. Dror, and D. E. Shaw. How fast-folding proteins fold. *Science*, 334(6055):517–520, 2011. doi: 10.1126/science.1208351. URL <https://www.science.org/doi/abs/10.1126/science.1208351>.
- A. D. J. MacKerell, D. Bashford, M. Bellott, R. L. J. Dunbrack, J. D. Evanseck, M. J. Field, S. Fischer, J. Gao, H. Guo, S. Ha, D. Joseph-McCarthy, L. Kuchnir, K. Kuczera, F. T. K. Lau, C. Mattos, S. Michnick, T. Ngo, D. T. Nguyen, B. Prodhom, W. E. Reiher, B. Roux, M. Schlenkrich, J. C. Smith, R. Stote, J. Straub, M. Watanabe, J. Wiórkiewicz-Kuczera, D. Yin, and M. Karplus. All-atom empirical potential for molecular modeling and dynamics studies of proteins. *The Journal of Physical Chemistry B*, 102(18):3586–3616, 1998. doi: 10.1021/jp973084f. URL <https://doi.org/10.1021/jp973084f>. PMID: 24889800.
- M. Neumann, J. Gin, B. Rhodes, S. Bennett, Z. Li, H. Choubisa, A. Hussey, and J. Godwin. Orb: A fast, scalable neural network potential, 2024. URL <https://arxiv.org/abs/2410.22570>.
- Y. Park, J. Kim, S. Hwang, and S. Han. Scalable parallel algorithm for graph neural network interatomic potentials in molecular dynamics simulations. *Journal of Chemical Theory and Computation*, 20(11):4857–4868, 2024. doi: 10.1021/acs.jctc.4c00190. URL <https://doi.org/10.1021/acs.jctc.4c00190>. PMID: 38813770.
- S. Passaro and C. L. Zitnick. Reducing so(3) convolutions to so(2) for efficient equivariant gnns. In *Proceedings of the 40th International Conference on Machine Learning*, ICML’23. JMLR.org, 2023.
- E. Qu and A. S. Krishnapriyan. The importance of being scalable: Improving the speed and accuracy of neural network interatomic potentials across chemical domains. In *The Thirty-eighth Annual Conference on Neural Information Processing Systems*, 2024. URL <https://openreview.net/forum?id=Y4mBaZu4vy>.
- W. Richards, T. Tsujimura, L. Miara, et al. Design and synthesis of the superionic conductor na10snp2s12. *Nature Communications*, 7:11009, 2016. doi: 10.1038/ncomms11009. URL <https://doi.org/10.1038/ncomms11009>.
- J. Riebesell, R. E. A. Goodall, P. Benner, Y. Chiang, B. Deng, G. Ceder, M. Asta, A. A. Lee, A. Jain, and K. A. Persson. Matbench discovery – a framework to evaluate machine learning crystal stability predictions, 2024. URL <https://arxiv.org/abs/2308.14920>.
- V. G. Satorras, E. Hoogeboom, and M. Welling. E(n) equivariant graph neural networks. *CoRR*, abs/2102.09844, 2021. URL <https://arxiv.org/abs/2102.09844>.

- K. T. Schütt, H. E. Sauceda, P.-J. Kindermans, A. Tkatchenko, and K.-R. Müller. SchNet – A deep learning architecture for molecules and materials. *The Journal of Chemical Physics*, 148(24): 241722, 03 2018. ISSN 0021-9606. doi: 10.1063/1.5019779. URL <https://doi.org/10.1063/1.5019779>.
- P. Shaw, J. Uszkoreit, and A. Vaswani. Self-attention with relative position representations. In *Proceedings of the 2018 Conference of the North American Chapter of the Association for Computational Linguistics: Human Language Technologies, Volume 2 (Short Papers)*. Association for Computational Linguistics, 2018.
- N. Shoghi, A. Kolluru, J. R. Kitchin, Z. W. Ulissi, C. L. Zitnick, and B. M. Wood. From molecules to materials: Pre-training large generalizable models for atomic property prediction, 2024. URL <https://arxiv.org/abs/2310.16802>.
- J. S. Smith, O. Isayev, and A. E. Roitberg. Ani-1: an extensible neural network potential with dft accuracy at force field computational cost. *Chemical science*, 8(4):3192–3203, 2017.
- J. Su, M. Ahmed, Y. Lu, S. Pan, W. Bo, and Y. Liu. Roformer: Enhanced transformer with rotary position embedding. *Neurocomputing*, 568:127063, 2024.
- N. Thomas, T. E. Smidt, S. Kearnes, L. Yang, L. Li, K. Kohlhoff, and P. Riley. Tensor field networks: Rotation- and translation-equivariant neural networks for 3d point clouds. *CoRR*, abs/1802.08219, 2018. URL <http://arxiv.org/abs/1802.08219>.
- H. Wang, L. Zhang, J. Han, and E. Weinan. Deepmd-kit: A deep learning package for many-body potential energy representation and molecular dynamics. *Computer Physics Communications*, 228: 178–184, 2018.
- H. C. Wang, S. Botti, and M. A. L. Marques. Predicting stable crystalline compounds using chemical similarity. *npj Computational Materials*, 7(1):12, 2021. doi: 10.1038/s41524-020-00481-6. URL <https://doi.org/10.1038/s41524-020-00481-6>.
- A. Wijesinghe and Q. Wang. A new perspective on "how graph neural networks go beyond weisfeiler-lehman?". In *International Conference on Learning Representations*, 2022. URL [https://openreview.net/forum?id=uxgg9o7bI\\_3](https://openreview.net/forum?id=uxgg9o7bI_3).
- K. Xu, W. Hu, J. Leskovec, and S. Jegelka. How powerful are graph neural networks?, 2019. URL <https://arxiv.org/abs/1810.00826>.
- P. Ying, A. Natan, O. Hod, and M. Urbakh. Effect of interlayer bonding on superlubric sliding of graphene contacts: A machine-learning potential study. *ACS Nano*, 18(14):10133–10141, 2024. doi: 10.1021/acsnano.3c13099. URL <https://doi.org/10.1021/acsnano.3c13099>. PMID: 38546136.
- D. Zhang, H. Bi, F. Z. Dai, et al. Pretraining of attention-based deep learning potential model for molecular simulation. *npj Computational Materials*, 10(94), 2024a. doi: 10.1038/s41524-024-01278-7. URL <https://doi.org/10.1038/s41524-024-01278-7>.
- D. Zhang, X. Liu, X. Zhang, et al. Dpa-2: A large atomic model as a multi-task learner. *npj Computational Materials*, 10:293, 2024b. doi: <https://doi.org/10.1038/s41524-024-01252-3>.

# Supplementary Information

## AlphaNet: Scaling Up Local Frame-based NNIP

### A Local Structures, Completeness, and Expressive Power of GNNs

Graph neural networks (GNNs) derive their **locality** from aggregating information within  $k$ -hop neighborhoods, typically limited to 1-hop interactions. While this design enables efficient learning, it inherently restricts their focus to local substructures such as trees, triangles, or cycles. These substructures define distinct **local isomorphism types**: (1) *Tree isomorphism*, where subgraphs share identical hierarchical parent-child relationships; (2) *Triangular isomorphism*, requiring matching cyclic triplets (e.g., molecular bond angles); and (3) *Subgraph isomorphism*, preserving node features and connectivity patterns.

The expressive power of permutation-invariant GNNs is classically evaluated via the 1-Weisfeiler-Lehman (1-WL) test (Xu et al., 2019). As established by (Wijesinghe and Wang, 2022), the 1-WL test is equivalent to a GNN’s capacity to discriminate *local subtree isomorphism*, measuring its ability to distinguish hierarchical neighborhood structures. However, this framework operates solely on 2D graph topologies, ignoring 3D geometric relationships (e.g., bond angles, torsional dihedrals), thereby failing to address molecular or material systems where spatial configurations are decisive.

**Completeness** in GNNs requires a transformation function  $f$  to satisfy  $f(X) = f(Y) \iff X$  and  $Y$  are isomorphic. We can extend completeness to **local geometric isomorphism**, where isomorphism is defined under 3D geometric constraints (distances, angles, chiralities). Concurrently, methods encoding 3D geometric invariants (Wijesinghe and Wang, 2022) have demonstrated enhanced expressivity, enabling differentiation of graphs with distinct local atomic environments beyond WL limitations. Similar to LeftNet (Du et al., 2023), AlphaNet is able to differentiate local structures beyond tree isomorphism by defining the 3D structure weights.

### B Experimental Details

#### B.1 Datasets

**The Defected Bilayer Graphene Dataset** (Ying et al., 2024) consists of reference structures specifically designed to train and validate machine learning potentials (MLPs). It includes three bilayer systems: V0V0 (pristine), V0V1 (single vacancy on the top layer), and V1V1 (single vacancy in both layers). The dataset comprises single-point DFT (PBE+MBD) energies and atomic forces calculated for various configurations, including different interlayer distances, stacking modes, and manually deformed structures. Additionally, snapshot configurations from MD simulations at different temperatures were included. The data were split into training, validation, and test sets, containing 3988, 4467, and 200 structures, respectively. Farthest point sampling (FPS) and principal component analysis (PCA) were used to ensure a representative and balanced division.

**The Formate Decomposition on Cu Dataset** (Batzner et al., 2022) consists of configurations related to the decomposition process of formate on a Cu surface, specifically involving the cleavage of the C-H bond. The dataset includes initial, intermediate, and final states, such as monodentate and bidentate formate on Cu  $\langle 110 \rangle$ , as well as the final state with an H ad-atom and desorbed CO<sub>2</sub> in the gas phase. Nudged elastic band (NEB) method (Henkelman et al., 2000) was used to generate an initial reaction path for the C-H bond breaking, followed by 12 short ab initio molecular dynamics (AIMD) simulations. These simulations were performed using the CP2K code, resulting in a total of 6855 DFT structures with a time step of 0.5 fs and 500 steps per trajectory. AlphaNet was trained on 2500 uniformly sampled structures from the full dataset, with a validation set of 250 structures and the mean absolute error evaluated on the remaining structures.

**The Zeolite Dataset** comprises essential reference structures designed for various applications such as catalysis, adsorption, and separation. Zeolites are highly valued porous materials that have been the subject of extensive scientific research due to their broad applicability. The dataset includes 16 distinct zeolites, with atomic-level trajectories obtained through *Ab Initio Molecular Dynamics* (AIMD) (Car and Parrinello, 1985) simulations conducted at 2000 K using the Vienna *Ab Initio Simulation Package* (VASP) (Kresse and Furthmüller, 1996; Kresse and Hafner, 1993). For each zeolite, 80,000 snapshots were extracted, and the corresponding energies and atomic forces were

calculated for every configuration. The dataset was randomly divided into training, validation, and test sets in a 6:2:2 ratio, comprising 48,000, 16,000, and 16,000 structures, respectively.

**The OC2M Dataset (Chanussot et al., 2021)** is a large-scale subset of the OC20 Dataset, specifically designed for training and evaluating machine learning models in the context of interatomic potentials. This dataset includes approximately 2 million atomic configurations in the training set, with validation and test sets containing 4 splits, which is In Domain (ID), out-of-domain adsorbate (OOD adsorbate), out-of-domain catalyst (OOD catalyst), and both of unseen adsorbate and unseen catalyst (OOD both). Each of them contains around 1 million structures. It encompasses configurations involving 56 different chemical elements, ensuring a broad and diverse representation of atomic environments. These configurations were generated using density functional theory (DFT) calculations, with a focus on a wide range of materials science applications, including bulk materials, surfaces, and defect structures. Originating from the comprehensive OC20 Dataset, the OC2M subset provides accurate total energies and atomic forces for each configuration. This extensive dataset is particularly valuable for developing and testing machine learning models that require a diverse and large-scale collection of training examples to achieve robust generalization across different types of atomic interactions.

**The MPTraj Dataset and Matbench Discovery Test (Riebesell et al., 2024).** MPTraj consists of 1,580,395 structures which are frames of the DFT relaxations performed on all 154,719 Materials Project materials (Deng et al., 2023). Matbench Discovery is a test task for predicting the stability of 256,963 materials, which is also known as WBM test set (Wang et al., 2021). In this case we train our model on the MPTraj dataset and test it on the WBM test set.

## B.2 Hyperparamters

Table 6: Hyperparameter configurations for five different datasets. Gra. denotes the defected graphene dataset, For. denotes the formate decomposition dataset, Zeo. denotes the zeolite dataset, OC2M denotes the OC2M dataset, MPTraj denotes the MPTraj dataset.

Parameter	Gra.	For.	Zeo.	OC2M	MPTraj
Learning rate (lr)	5e-4	5e-4	5e-4	1e-4	1e-4
Scheduler	Cos.	Cos.	Cos.	Cos.	Cos.
Epochs	150	150	100	130	200
Loss func.	MAE	MAE	MAE	MAE	MAE
Batch size (per device)	24	12	96	4	12
Num layers	3	3	3	4	6
Heads	16	16	16	16	24
Num basis	32	32	32	96	256
Hidden channels	128	128	128	256	256
Cutoff (Å)	5	5	5	5	6

## B.3 Training cost on the OC2M dataset and MPTraj

Table 7: Training cost for the OC2M and MPTraj datasets. The training memory here is determined by dividing the fixed memory capacity of a GPU by the batch size.

Dataset	Training Time (GPU Days)	Number of Parameters	Training Memory (GB per sample)
OC2M	361	6.1M	5.1
MPTraj	243	16.2M	10.1

## B.4 Baseline Models

For computational modeling configurations, NequIP achieves optimal performance with tensor rank 2, feature size 32, and 5 Å cutoff in the formate decomposition dataset, while using tensor rank 1 with 7 Å cutoff for defective graphene studies. The zeolite dataset employs a fine-tuned DPA-2 potential via Deep Pot implementation ((Zhang et al., 2024b)). Models trained on OC20 leverage pre-trained SchNet/DimeNet++ architectures from <https://fair-chem.github.io/>

[core/model\\_checkpoints.html](#), with other results cross-validated against (Qu and Krishnapriyan, 2024) using publicly accessible validation sets. MPtrj benchmark data integrates results from <https://matbench-discovery.materialsproject.org/> and comparative analysis in (Qu and Krishnapriyan, 2024). Speed testing on zeolite structures maintains uniform 2-layer architectures with 5 Å cutoff, where PaiNN/SchNet employ 120-atom basis and 16 RBF basis, MACE uses tensor order 0-1 (feature size 16), NequIP extends to tensor order 0-2 (feature size 16), AlphaNet configures 32 hidden channels with 12 attention heads, and EquiformerV2 implements sphere/edge channels 16 with 16-dimensional attention hidden states and 2-head mechanisms.

## C Ablation Study

Table 8: Ablation study on the impact of RoPE, temporal connections (Temp Connect), and frame transition encoding (FTE).

Configuration	Energy (meV/atom) ↓	Force MAE (meV/Å) ↓
Full Model	1.7	32.0
w/o RoPE	25.9	113.6
w/o Temp Connect	2.9	38.2
w/o FTE	2.8	45.3

We do ablation study on the Defected Graphene dataset, Table 8 shows that all the component matters, but it is worth notice that our model can not get down the loss and performs bad with out RoPE, though this did not happen in our other tests. While shows that RoPE is important, some other aspects may need to be considered such as more efficient way of optimizing tensor network.

## D Data Scaling and Dynamic loss weights

The experimental datasets were generated using *VASP* (Kresse and Furthmüller, 1996; Kresse and Hafner, 1993), where the energy per atom typically converges around 5 eV under our default training settings. These configurations demonstrated robust performance within this energy regime. However, when applied to systems with significantly higher energy magnitudes per atom and greater energy variance—such as those produced by *CP2K* (Kühne et al., 2020) simulations—the original settings failed to achieve stable convergence. To address this challenge, we developed a dynamic optimization strategy: initially adjusting the energy-to-force loss weight ratio from  $\lambda_E : \lambda_F = 4 : 100$  to  $0.05 : 100$ , then progressively increasing  $\lambda_E$  while simultaneously decaying the learning rate. This coordinated adaptation proved critical for successful training in high-variance scenarios.